

Two-dimensional electron gas in a metal/amorphous oxide interface with spin orbit interaction

J.M. Flores-Camacho,^{1,*} Jorge Puebla,^{2,†} Florent Auvray,^{2,3} Yoshichika Otani,^{2,3} and R.E. Balderas-Navarro¹

¹ Instituto de Investigación en Comunicación Óptica,
Universidad Autónoma de San Luis Potosí, Álvaro Obregón 64, 78000 San Luis Potosí, Mexico

² Center for Emergent Matter Science, RIKEN, Wako, Saitama 351-0198, Japan

³ Institute for Solid State Physics, University of Tokio, Kashiwa, Chiba 277-8581, Japan

(Dated: December 15, 2024)

The formation of novel two-dimensional electron gas (2DEG) with high mobility in metal/amorphous interfaces has motivated an ongoing debate regarding the formation and novel characteristics of these 2DEGs. Here we report an optical study, based on spectroscopic ellipsometry, of nonmagnetic metal and amorphous semiconducting oxide ($\text{Cu}/\text{Bi}_2\text{O}_3$) interfaces that confirms the formation of a 2DEG with spin orbit coupling (SOC). In addition we detect Fano resonances which are attributed to the coupling of 2DEG quantum confined states with the continuum of the interface-bulk states. In particular, the line shape of the interfacial 2DEG dielectric function (DF) thus resolved in Drude and Lorentz components resulted very similar to theoretical predictions [M. Xie *et al.*, Phys. Rev. B **89**, 245417 (2014)] of a two dimensional electron gas confined in the normal direction of a perovskite interface. Although the original constituent materials do not possess spin-orbit coupling (SOC), the resulting interfacial hybridization of such states induce electronic asymmetric wave functions. This work demonstrates the detection of 2DEG in amorphous crystals allowing to study its challenging interfacial phenomena such as SOC and interface-bulk coupling, overcoming an experimental impediment which has hold back for decades important advancements for the understanding of 2DEGs in amorphous materials.

PACS numbers: 78.68.+m, 73.20.r, 73.40.-c, 71.70.Ej

The concept of two-dimensional electron gas (2DEG) has contributed enormously to the understanding of the rich phenomena of electrons confined at surfaces and interfaces. In high quality semiconductor heterostructures, 2DEG confinement induced enhancement of electron mobility leading to technology advancements and scientific discoveries, such as the fractional Quantum Hall effect [1]. The continuous development of growth techniques allows nowadays to obtain enough good quality heterostructures from oxides, forming novel 2DEGs. Interestingly, 2DEG in oxides show a significant increase in electron density and strong electron correlation, with consequences in magnetic properties, superconductivity, ferroelectricity and spin orbit interaction [2, 3]. Intrinsically, the electronic structure of 2DEG in oxide interfaces is different from the most standard semiconductor counterparts. In most of the oxide interfaces, the transport properties are dominated by narrow d -band electrons, whereas in semiconductors the electrons localized at states at the bottom of the conduction band dictate the properties of the 2DEGs. However, despite of the great advance in the understanding of 2DEG in complex oxide interfaces, still many oxide interfaces are challenging to characterize, mainly because their crystal quality. Analysis of the electronic structure is commonly achieved by angle-resolved photoemission spectroscopy (ARPES). However, ARPES characterization requires high quality, large and flat crystals. For instance, high quality crystals of bismuthates were obtained, allowing detailed characterization by ARPES and revealing the mechanism of its

high temperature superconductivity, an open discussion for more than 30 years [4].

Moreover, the formation of novel 2DEG with high mobility in amorphous oxides has motivated an increasing interest [5, 6]. The origin of the 2DEG formation at these interfaces has been assigned to electronic reconstruction via interfacial charge transfer [7]; however, detailed characterization of the properties of 2DEGs formed by amorphous oxides is still lacking. An alternative to ARPES characterization is to analyze optical conductivity of the 2DEGs by polarized spectroscopy techniques such as spectroscopic ellipsometry. Although, structural distortion and defects in amorphous materials may cause complex dielectric screening, and significantly complicate the analysis of the properties of the 2DEG, a theoretical model can be assessed and improved by direct feedback from optical characterization [8].

Here, we report on infrared ellipsometry characterization of the properties of 2DEG formed at the interface between a nonmagnetic metal and amorphous semiconducting oxide, $\text{Cu}/\text{Bi}_2\text{O}_3$. Recent spin-charge interconversion experiments suggest the presence of a 2DEG with spin orbit coupling (SOC) at this interface [9–11], making it a very attractive structure for spin based complementary metal-oxide semiconductor technologies (CMOS) [12, 13]. The characterization by angle resolved ellipsometry confirms the formation of a 2DEG with SOC. In-depth analysis of the optical conductivity, modeled by a realistic electronic structure system and Kubo formalism, allows to define the origin of SOC as the hybridization of inter-

facial Cu-O-Bi states by charge transfer, generating an asymmetric wave function [11], as previously suggested for amorphous perovskite oxides [6, 7]. We resolve the Drude and Lorentz contributions and obtain the 2DEG resistivity ρ_0 , relaxation time τ_e and describe the 2DEG SOC strength Δ_{SOC} . Furthermore, we observe a Fano resonance which describes the coupling of oxygen vacancies [14–17] shallow trap states to the 2DEG continuum of the interface-bulk transition. This work allows assessing the complex phenomena associated to the presence of 2DEG, SOC and Fano resonance at interfaces between amorphous crystals. Beyond the particular case of study in the present letter, the supporting theoretical model [8] and advance ellipsometry technique suggests applicability in a larger range of unexplored amorphous interfaces.

The samples consist of Bi_2O_3 films, with thickness of 20 nm, grown on a previously (10, 20, and 50 nm thick) Cu-capped $\text{SiO}_2/\text{Si}(001)$ substrate as described elsewhere [9, 18]. The structure is shown in Fig. 1(a). Additionally, in order to contrast the presence of 2DEG and for obtaining the dielectric function (DF) of thin Cu film alone, a second set of reference samples were prepared as shown in Fig. 1(b).

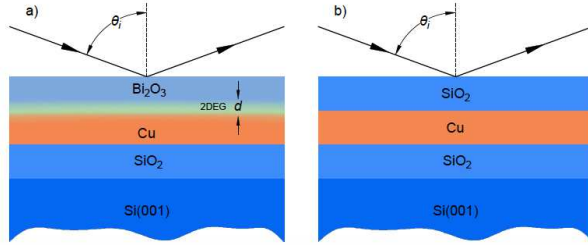


FIG. 1. Diagrams of the samples used for the ellipsometry measurements at angles of incidence θ_i . (a) sample comprising 20 nm Bi_2O_3 film deposited on top of a Cu (either 10, 20, or 50 nm thick)/ SiO_2 (320 nm)/ $\text{Si}(001)$ substrate. The 2DEG formed upon deposition of the Bi_2O_3 film is depicted with thickness d . (b) reference sample with SiO_2 instead of Bi_2O_3 .

The samples were characterized by infrared spectroscopic ellipsometry (IRSE) by means of an IR-VASE apparatus (J.A. Woollam Co.). Ellipsometry measures the change in polarization state upon oblique reflection of an originally linear polarized incident beam [19]. The reflected state of polarization is measured by the complex ratio $r_p/r_s = \tan \psi \exp(i\Delta)$, where r_p and r_s are the complex reflection coefficients for p and s polarizations of light, standing for parallel and perpendicular to the plane of incidence, respectively. The ellipsometric angles ψ and Δ measure then the relative change of amplitude and phase, respectively, of the p to s polarizations [20]. Mid-infrared SE was measured in the range of ~ 35 to 760 meV in ambient conditions.

The total reflection coefficients are calculated separately for s and p polarizations using Fresnel coefficients consisting of a model of 6 stacked media: (0) vacuum,

(1) 20 nm Bi_2O_3 , (2) an interfacial layer to accommodate the 2DEG, (3) Cu thin film, (4) 320 nm SiO_2 , and (4) Si substrate [see Fig. 1(a)] [21]. It is important to note that attempts made without the artificially introduced 2DEG layer failed to simulate the main features of the experimental curve. However, it worked nicely for the Cu/ SiO_2 reference samples, as shown in Fig. 2(c) and (d), indicating that the interfacial layer must be necessarily included for the Cu/ Bi_2O_3 samples.

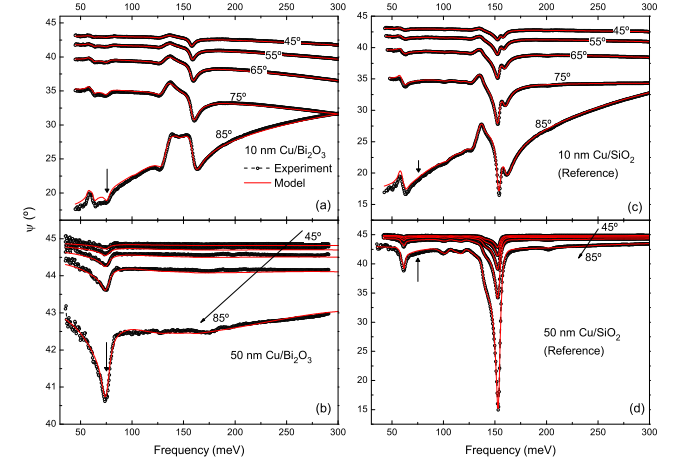


FIG. 2. (Color online) Experimental (symbols) and calculated (lines) ψ spectra recorded at different angles of incidence (indicated) corresponding to (left) the Bi_2O_3 on (a) 10 nm Cu and (b) 50 nm Cu, and (right) to the Cu/ SiO_2 reference samples (c and d). The vertical arrows at ~ 76 meV indicate the position of a Fano resonance detected at the Cu/ Bi_2O_3 interfaces.

The DF of each layer is parameterized as a sum of oscillators, which for the case of the interfacial layer can be written as

$$\varepsilon(\omega) = \varepsilon_{\infty} + \varepsilon_D(\omega) + \varepsilon_F(\omega) + \sum_i \varepsilon_{L,i}(\omega), \quad (1)$$

where $\varepsilon_D(\omega)$ is the Drude term contributed by the free electron gas, the $\varepsilon_{L,i}(\omega)$ terms are used to include responses within the measured spectral range, commonly a Lorentz function. ε_{∞} is a (real) constant offset. In Eq. (1) we have included a Fano resonance, ε_F , given by [22]

$$\varepsilon_F(\omega) = A(q) \left(\frac{(q^2 - 1)\Delta\omega + 2q}{\Delta\omega^2 + 1} + i \frac{(q - \Delta\omega)^2}{\Delta\omega^2 + 1} \right), \quad (2)$$

where q is the Fano parameter which, concerning only the line shape, governs the oscillator strength $A(q)$ and phase [23, 24], $\Delta\omega = (\omega_0 - \omega)/\Gamma$, with ω_F and Γ_F being the Fano resonance frequency and broadening, respectively. The DFs of bulk-like Bi_2O_3 and Cu of 10, 20, and 50 nm, shown in the Supplementary Mater Section, were obtained from reference samples. The bulk DF of Cu cannot be used for our models since for the

present thicknesses the Cu layer is still near the percolation threshold [25–27]. The DF of the Cu layer was parameterized with a Drude-modified model [28], but it returned essentially a classical Drude line shape with diminished conductivity (See Fig. S3).

The substrate Si/SiO₂, and the Si/SiO₂/Bi₂O₃ reference samples were fitted with VASE32, obtaining thus the thickness of the thermally grown SiO₂ of 322 nm, which is used for all subsequent samples, and the mid-infrared *pristine* Bi₂O₃ DF. α -Bi₂O₃ has a series of small phonons in this spectral region below 66 meV [29, 30], which were not detected in our experiment. Also, the group of features at \sim 60 and 150 meV in Fig. 2(a), (c), and (d) correspond to SiO₂ and their strengths can be therefore used as a measure of the spectral absorption of the Cu layer in the samples containing it. For the Cu/SiO₂ spectra, shown in Fig. 2(c) and (d), the dips are easily reproduced by the model without great effort. A further utilization of the reference samples consisted on trying to emulate artificially the presence of a 2DEG-like intermediate layer in order to verify whether the Cu/Bi₂O₃ model was real or an artifact: In Cu/SiO₂ the artificial layer resulted on either “pure” SiO₂, Cu or an effective medium-like combination of both, depending on the placement of the artificial layer (see Fig. S7 and its discussion).

Experimental and calculated ψ spectra for Cu/Bi₂O₃ recorded at different angles of incidence are shown in Fig. 2(a) and (b). The overall spectra are dominated by Cu reflectivity and its corresponding thickness-dependent optical conductivity. In both cases, a feature modeled as a combination of a Lorentz and Fano resonances is observed at energies \leq 76 meV, which are attributed to characteristics of the 2DEG interfacial layer as described below.

The overall resulting optical conductivities $\sigma(\omega)$ of the Cu/Bi₂O₃ interface are presented in Fig. 3. It is observed that $\sigma(\omega)$ depends on the underlying Cu film thickness. This dependence can be explained in terms of modulation of charge transfer to the Bi₂O₃ due to the mobility of electrons within the Cu layer itself: for thicknesses below 20 nm, the layer is below its percolation threshold, which implies the formation potential barriers within the layer and consequently modified work functions. Indeed, it has been reported that the relation of work functions of the materials at the interface are critical for the resulting characteristics, like the relative occupancy of hybridized orbitals near the interface [14], of the 2DEG at the Bi₂O₃ on non-magnetic metals interfaces [11] and perovskite oxide-oxide interfaces [6].

The new layer, in contrast to the aforementioned Cu/SiO₂ experiments, resulted in strong optical spectral features quite different from those of the original constituent materials. Strikingly, the line shape of the interfacial layer DF thus resolved in Drude and Lorentz components, resulted very similar to theoretical predic-

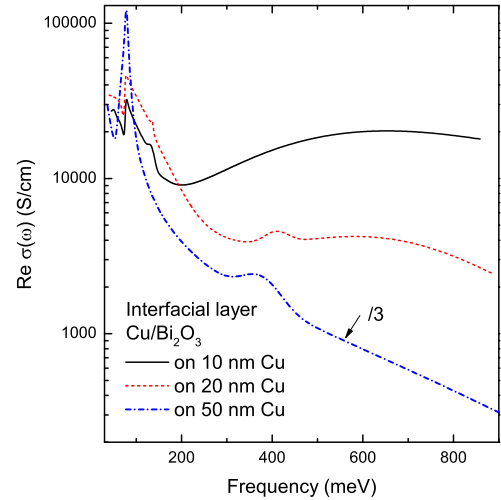


FIG. 3. Real part of the optical conductivity of the interfacial layer forming between Bi₂O₃ and Cu as extracted from the fitting procedure for the samples with Cu layer thickness of 10, 20, and 50 nm.

tions [8] of a two dimensional electron gas confined in the normal direction of the system. The hybridization of interfacial orbital states induce electronic asymmetric wave functions, in contrast with the original constituent materials which do not possess SOC. Such asymmetric wave functions thus induce an interfacial electric field suggesting SOC of the Rashba type [31, 32]. This statement is in agreement with first-principle calculations recently reported for Cu/Bi₂O₃ [11, 33].

As we are only considering isotropic DFs for all layers, it brings as a consequence a fitting error that grows with increasing angle of incidence. This hints to the presence of anisotropic DFs ($\varepsilon_{xx} = \varepsilon_{yy} \neq \varepsilon_{zz}$) as predicted in Ref. [8].

In the following we describe the distinct contributions of the total conductivity shown in Fig. 3. First, the 2DEG optical conductivity associated to a Drude (free-electron) line shape. This is presented in Fig. 4 as $\text{Re}(\sigma)$ and its most relevant parameters, DC resistivity ρ_0 , and mean time of life τ_e as functions of underlying Cu thickness in Table I. It is observed that while ρ_0 decreases quasi-linearly with increasing Cu thickness, τ_e seems to increase although non monotonically, and can be associated to an additional interfacial build-up strain [34].

In Table I we also report on the thickness of the 2DEG layer, d . This number provided minimization of error in the present interface model, however, this does not preclude some extension of the effect further in z -direction as observed in Ref. [35].

The rest of the most relevant interfacial layer spectral features are presented in two separate spectral regions due to large differences in amplitude. Since two of the resonances are consistent with theoretical predictions [8], concerning their relative amplitudes and the behavior of

TABLE I. Relevant parameters of the interfacial 2DEG layer depending on underlying Cu thickness t_{Cu} . d is the 2DEG thickness, ρ_0 and τ_e are DC resistivity and relaxation lifetime of the Drude contribution. q , ω_F , and Γ_F are center frequency, and broadening of the Fano resonance; q is the Fano-factor. ω_i and γ_i ($i = (1, 2)$) are SOC _{i} center and broadening, respectively.

t_{Cu} (nm)	d (nm)	Drude		Fano		Γ_F (meV)	SOC1		SOC2	
		ρ_0 (10^{-5} $\Omega\cdot\text{cm}$)	τ_e (fs)	q	ω_F (meV)		ω_1 (meV)	γ_1 (meV)	ω_2 (meV)	γ_2 (meV)
10	2.21	3.3	9.2	1.19	76.1	3.4	54.4	105.0	—	—
20	2.85	2.59	9.0	1.0	74.7	3.4	70.0	71.4	408	61.2
50	3.20	0.42	18.2	8.5	77.0	4.0	69.9	31.1	398	101.2

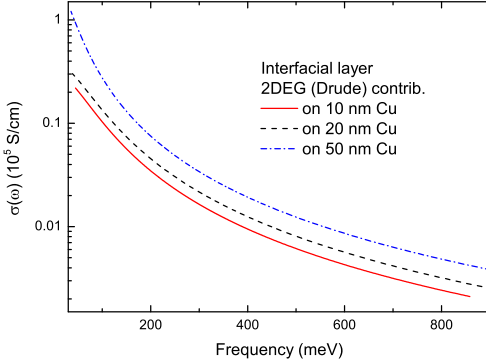


FIG. 4. (Color online) Real part of the Drude contribution to the total optical conductivity of the 2DEG forming in the interfacial layer.

their shifts and strength as a function of (Cu-provided) charge density, we will regard them as SOC₁ and SOC₂ for their energy positions, respectively. In Fig. 5 we present the orbital hybridization allowed [8] SOC₁ resonance (solid line), which notably increases in strength as function of available charge in the interfacial layer, whereas its shifting position (to higher energies) seems to come to a stop for underlying Cu thickness above 20 nm. We have associated the sharp feature at ~ 76 meV with a Fano resonance [36] for which, in the present work, might reflect the coupling of the 2DEG continuum with the discrete states produced by oxygen vacancies [7, 14, 17] that very likely form near the $\alpha\text{-Bi}_2\text{O}_3$ conduction band as well, facilitated by its bulk-like energy structure [37]. This is to be contrasted with a Berreman resonance [38] observed at the polar-nonpolar oxide-oxide interface produced by the presence of the 2DEG [14, 35] when the real part of DFs at both sides coincide. We clearly have not the condition to fulfill this criterion.

At higher frequencies there are two (uncoupled) broad features. A very broad one covering most of the plotted region (dashed lines in Fig. 6) that tends to decrease in amplitude and shifts to higher energies as a function of the underlying Cu thickness, and is consistent with phenomenological percolation theories producing a mid-infrared broad peak, which in turn manifests electronic collisions accompanying the main Drude feature, and predict a recovery of the usual free-electron gas behavior

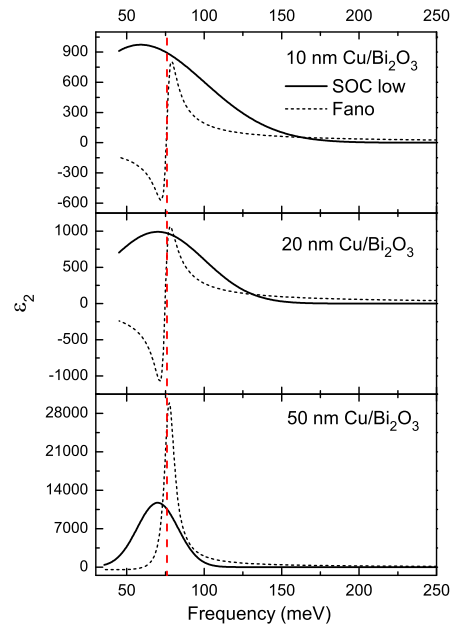


FIG. 5. Spin-orbit coupling (SOC) contributions to the optical conductivity of the interfacial layer, in ϵ_2 representation, corresponding to the indicated Cu film thicknesses. A broad feature (solid lines), the proper low energy SOC, shifts to higher frequencies and increases in strength as a function of the underlying Cu film thickness. In the same spectral region, a sharp Fano resonance (dashed lines) also increases but does not show substantial shift; only its Fano factor q is modified with increasing Cu thickness.

as the percolation threshold is surpassed [28]. A second structure, called SOC₂, detected only for the thicker Cu samples, does the opposite: increases and shifts to lower frequencies (solid lines in Fig. 6). The behavior of amplitude ratios, broadening, and energy positions of SOC₂ and SOC₁ in Fig. 5, are consistent with the trend predicted for intersubbands optical response as a function of carrier density at the 2DEG [8].

In summary, we have detected the presence of a 2DEG at the interface of an amorphous oxide with a non magnetic metal by means of infrared ellipsometry. Beside the substrate dependent carrier density free-electron (Drude-like) behavior, we have also observed intersubband features consistent with SOC of the Rashba type. Furthermore, a Fano resonance that can be attributed to the

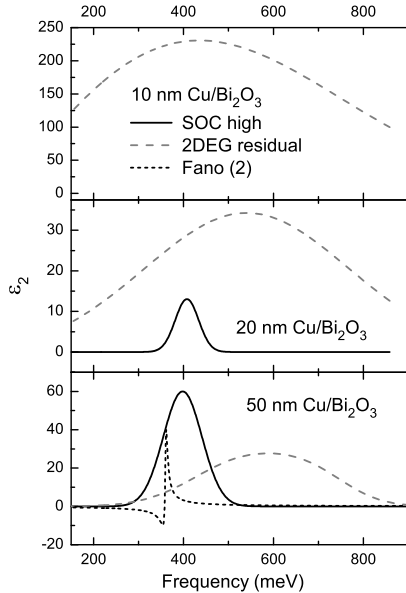


FIG. 6. Higher energy SOC contribution to the interfacial layer total response (solid lines). A broader feature that shifts to higher frequencies and decreases with increasing underlying Cu thickness is also detected in this region. The latter can be explained in terms of collisions of the 2DEG electrons. For 10 nm Cu, the SOC contribution is below detection and thus not reported here.

coupling of the 2DEG continuum with oxygen vacancies discrete states has also been detected. The present report sheds light on the complex phenomena at amorphous interfaces that have been elusive for decades.

We thank Prof. A. H. MacDonald (University of Texas at Austin) and Prof. J. J. Palacios (Universidad Autónoma de Madrid) for insightful guidance. We also thank Consejo Nacional de Ciencia y Tecnología (Mexico) for Grants Nos. CB-252867-2015 and 206298. This work was also supported by a Grant-in-Aid for Scientific Research on Innovative Area, “Nano Spin Conversion Science” (Grant No. 26103002) and RIKEN incentive Research Project Grant No. FY2016.

* e-mail (JMFC): jmflores@actus.iico.uaslp.mx
 † e-mail (JP): jorgeluis.pueblanunez@riken.jp

[1] H. L. Stormer, D. C. Tsui, and A. C. Gossard, *Rev. Mod. Phys.* **71**, S298 (1999).
 [2] J. Mannhart and D. G. Schlom, *Science* **327**, 1607 (2010).
 [3] H. Y. Hwang, Y. Iwasa, M. Kawasaki, B. Keimer, N. Nagaosa, and Y. Tokura, *Nature Materials* **11**, 103 (2012).
 [4] C. H. P. Wen, H. C. Xu, Q. Yao, R. Peng, X. H. Niu, Q. Y. Chen, Z. T. Liu, D. Shen, Q. Song, X. Lou, et al., *Phys. Rev. Lett.* **121**, 117002 (2018).
 [5] S. W. Lee, Y. Liu, J. Heo, and R. G. Gordon, *Nano Lett.* **12**, 4775 (2012).
 [6] Y. Chen, F. Trier, T. Wijnands, R. J. Green, N. Gauquelin, R. Egoavil, D. V. Christensen, G. Koster, M. Huijben, N. Bovet, et al., *Nat. Mat.* **14**, 801 (2015).
 [7] Z. Q. Liu, C. J. Li, W. M. Lü, X. H. Huang, Z. Huang, S. W. Zeng, X. P. Qiu, L. S. Huang, A. Annadi, J. S. Chen, et al., *Phys. Rev. X* **3**, 021010 (2013).
 [8] M. Xie, G. Khalsa, and A. H. MacDonald, *Phys. Rev. B* **89**, 245417 (2014).
 [9] J. Puebla, F. Auvray, M. Xu, B. Rana, A. Albouy, H. Tsai, K. Kondou, G. Tatara, and Y. Otani, *Appl. Phys. Lett.* **111**, 092402 (2017).
 [10] M. Xu, J. Puebla, F. Auvray, B. Rana, K. Kondou, and Y. Otani, *Phys. Rev. B* **97(18)**, 180301 (2018).
 [11] H. Tsai, S. Karube, K. Kondou, N. Yamaguchi, F. Ishii, and Y. Otani, *Sci. Rep.* **8**, 5564 (2018).
 [12] S. Manipatruni, D. E. Nikonov, and I. A. Young, *Nat. Phys.* **14**, 338 (2018).
 [13] S. Manipatruni, D. E. Nikonov, C.-C. Lin, T. A. Gosavi, H. Liu, B. Prasad, Y.-L. Huang, E. Bonturim, R. Ramesh, and I. A. Young, *Nature* **565**, 35 (2019).
 [14] S. Y. Park and A. J. Millis, *Phys. Rev. B* **87**, 205145 (2013).
 [15] M. Yazdi-Rizi, P. Marsik, B. P. P. Mallet, A. Dubroka, D. V. Christensen, Y. Z. Chen, N. Pryds, and C. Bernhard, *Eur. Phys. Lett.* **113**, 47005 (2016).
 [16] P. Torruella, C. Coll, G. Martín, L. López-Coneza, M. Vila, C. Díaz-Guerra, M. Varela, M. L. Ruiz-González, J. Piqueras, F. Peiró, et al., *J. Phys. Chem. C* **121**, 24809 (2017).
 [17] C.-J. Li, Y.-P. Hong, H.-X. Xue, X.-X. Wang, Y. Li, K. Liu, W. Jiang, M. Liu, L. He, R.-F. Dou, et al., *Sci. Rep.* **8**, 404 (2018).
 [18] F. Auvray, J. Puebla, M. Xu, B. Rana, D. Hashizume, and Y. Otani, *J Mater Sci: Mater Electron* **29**, 15664 (2018).
 [19] R. M. A. Azzam and N. M. Bashara, *Ellipsometry and polarized light* (North-Holland, Amsterdam, 1977).
 [20] J. Humlíček, in *Handbook of ellipsometry*, edited by H. G. Tompkins and E. A. Irene (William Andrew, Springer, New York, Heidelberg, 2005), p. 3.
 [21] O. S. Heavens, *Optical properties of thin solid films*, Dover classics of science and mathematics (Dover, New York, 1995).
 [22] M. V. Marquezini, P. Kner, S. Bar-Ad, J. Tignon, and D. S. Chemla, *Phys. Rev. B* **57**, 3745 (1998).
 [23] M. F. Limonov, M. V. Rybin, A. N. Poddubny, and Y. S. Kivshar, *Nat. Photonics* **11**, 543 (2017).
 [24] B. Luk'yanchuk, N. I. Zheludev, S. A. Maier, N. J. Halas, P. Nordlander, H. Giessen, and C. T. Chong, *Nat. Materials* **9**, 707 (2010).
 [25] M. Hövel, B. Gompf, and M. Dressel, *Phys. Rev. B* **81**, 035402 (2010).
 [26] H. Lee, H. Lee, J.-H. Park, H.-K. Kim, B. H. Kong, and H. K. Cho, *Jap. J. Appl. Phys.* **50**, 055805 (2011).
 [27] T. V. Amotchkina, V. Janicki, J. Sancho-Parramon, A. V. Tikhonravov, M. K. Trubetskov, and H. Zorc, *Appl. Opt.* **50**, 1453 (11).
 [28] N. Smith, *Phys. Rev. B* **64**, 155106 (2001).
 [29] S. N. Narang, N. D. Patel, and V. B. Kartha, *J. Mol. Struct.* **327**, 221 (1994).
 [30] A. B. Kuzmenko, E. A. Tishchenko, I. L. Sashin, M. N. Khlopkin, and V. G. Orlov, *J. Low Temp. Phys.* **105**, 861 (1996).
 [31] Y. A. Bychov and E. I. Rashba, *Pis'ma Zh. Eksp. Teor. Fiz.* **39**, 66 (1984).

- [32] A. Manchon, H. C. Koo, J. Nitta, S. M. Frolov, and R. A. Duine, *Nat. Materials* **14**, 871 (2015).
- [33] J. Puebla, F. Auvray, N. Yamaguchi, M. Xu, S. Bisri, Y. Iwasa, F. Ishii, and Y. Otani, arXiv:1902.00237 (2019).
- [34] L. D. Sun, M. Hohage, P. Zeppenfeld, R. E. Balderas-Navarro, and K. Hingerl, *Phys. Rev. Lett.* **96**, 016105 (2006).
- [35] A. Dubroka, M. Rössle, K. W. Kim, V. K. Malik, L. Schultz, S. Thiel, C. W. Schneider, J. Mannhart, G. Herranz, O. Copie, et al., *Phys. Rev. Lett.* **104**, 156807 (2010).
- [36] U. Fano, *Phys. Rev.* **124**, 1866 (1961).
- [37] A. Walsh, G. W. Watson, D. J. Payne, R. G. Edgell, J. Guo, P.-A. Glans, T. Learmonth, and K. E. Smith, *Phys. Rev. B* **73**, 235104 (2006).
- [38] B. W. Berreman, *Phys. Rev.* **130**, 2193 (1963).

Supplemental Information: Two-dimensional electron gas in a metal/amorphous oxide interface with spin orbit interaction

J. M. Flores-Camacho,^{1,*} Jorge Puebla,^{2,†} Florent Auvray,^{2,3} Yoshichika Otani,^{2,3} and R. E. Balderas-Navarro¹

¹ Instituto de Investigación en Comunicación Óptica,
Universidad Autónoma de San Luis Potosí, Álvaro Obregón 64, 78000 San Luis Potosí, Mexico

² Center for Emergent Matter Science, RIKEN, Wako, Saitama 351-0198, Japan

³ Institute for Solid State Physics, University of Tokio, Kashiwa, Chiba 277-8581, Japan

(Dated: December 15, 2024)

SUPPLEMENTAL INFORMATION

Substrate and pristine Bi_2O_3

The substrate for all samples is a 320 nm thick thermally grown SiO_2 layer on $\text{Si}(001)$ wafer. Since intrinsic Si is transparent in the present spectral range (30 - 800 meV), spurious partially-incoherent signals from light reflected off the back side could reach the detector. Therefore, a sandblasting treatment was applied to all samples backsides, obtaining thus a surface rough enough that all light is scattered. In this way only the relevant signals from the overayers grown on the first surface can be acquired by the instrument's detector. Both transmission and depolarization measurements were made to test the success of the treatment. Transmission turned out to be negligible, whereas the loss of polarization resulted in near zero values except measurements at angle of incidence of 85° , for which the depolarization is below 2.5% for all Cu containing samples.

Ellipsometry data from the SiO_2/Si reference sample (from now on, the substrate) was fitted with Si and SiO_2 parametrized dielectric functions included in the VASE32[©] software database (see dash-dotted line in Fig. S1). In this case, the only fitting parameter was the SiO_2 thickness, which resulted in 322.5 ± 0.50 nm. The employed parametrized Si dielectric function is a Drude-type line shape consistent with a doping of $n = 3.54 \times 10^{15} \text{ cm}^{-3}$. The optical model of this sample works as the base for the fitting procedure of all subsequent samples, i.e., in the following we assume that the substrate is the same for all models.

A reference sample was prepared with the purpose of determining the dielectric function of bulk-like Bi_2O_3 . In the model, the substrate contributions was taken unaltered from the previously fitted reference substrate. Indeed the sharp features below 200 meV seen in almost all raw spectra, are originated from the SiO_2 thermal oxide layer. For the Bi_2O_3 film we determined that its dielectric function is the one shown in Fig. S2. A film thickness of 19 nm resulted from the fit, which is quite consistent with the nominal value of 20 nm. In this stage we are more interested in obtaining dielectric functions that could be used for the working samples. As discussed below, the Bi_2O_3 film thickness was left as parameter for

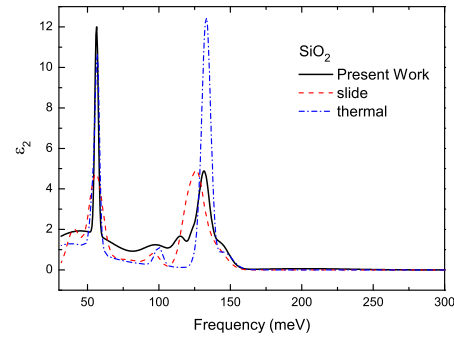


FIG. S1. Imaginary part of the SiO_2 dielectric function as extracted from the present work reference samples (solid line) are shown together with data from a thermally grown SiO_2 on Si (dash-dotted line) and of a microscope slide glass.

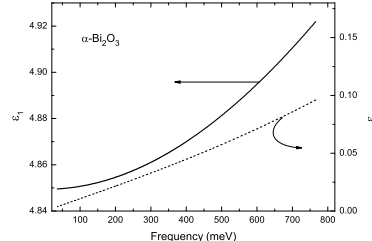


FIG. S2. Dielectric function of $\alpha\text{-Bi}_2\text{O}_3$ extracted from model of reference samples consisting on $\text{Bi}_2\text{O}_3/300$ nm SiO_2/Si .

the Cu samples: possibly due to different sticking coefficients the Bi_2O_3 thickness suffered a small variation from sample to sample (19.0 to 23.0 nm).

For the fitting procedure we employed VIS-UV data from literature as reference data for the high energy side of the mid-infrared, from where a point by point pre-fit was initiated. To ensure Kramers-Kronig consistency the pre-fit was parametrized with Lorentz and Tauc-Lorentz oscillators. It is reported that Bi_2O_3 has a finite DC conductivity, which could be implemented by a Drude line shape. However, inclusion of this line shape did not reflect improvement on the low energy side of the spectrum and was thus excluded in order to preserve simplicity. Furthermore, Bi_2O_3 has a multitude of small vibrational-related peaks below 76 meV, which were also ruled out since the ellipsometer was not able to detect them.

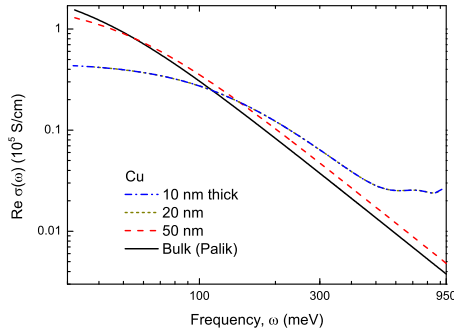


FIG. S3. Real part of the thickness dependent Cu optical conductivity $\sigma(\omega)$ as extracted from $\text{SiO}_2/\text{Cu}/\text{SiO}_2/\text{Si}$ reference samples. Bulk Cu optical conductivity calculated from tabulated data [3] is shown for comparison.

Cu optical constants

The dielectric function of the Cu layer was approximated by employing the Drude-Smith model. This is justified by the fact that a thin metallic layer is close to the percolation threshold [1, 2]. TEM images show that the Cu layer is already quite continuous (a manuscript is in preparation), which precludes us from considering a particulate medium, however, the grain boundaries may still be of great influence. A rough medium composed of $\alpha\text{-Bi}_2\text{O}_3$ and Cu can also be ruled out. A possible phase of cooper oxides can be considered, however, the characteristic infrared peaks of these oxides were not observed in the experiment. Furthermore, in order to justify the employment of a dielectric function with a Drude-Smith line shape with low conductivity instead of the bulk-like dielectric function arises by the experimental observation that the infrared peaks of SiO_2 beneath the Cu layer are not quenched as it would occur had the 10 nm thick Cu possessed already bulk properties. The resulting real part of the thickness dependent Cu optical conductivity is shown in Fig. S3, where comparison with tabulated bulk data from standard literature [3] is also shown.

Reference samples Cu/ SiO_2 fits

The Cu/ SiO_2 samples, whose best fits are shown in Fig. S4, were used with a two-fold purpose: first, as references to obtain the thickness dependent dielectric function of the near percolation threshold Cu layer, and second, to test our Cu/ Bi_2O_3 model against the possibility of a false-positive of the presence of the 2DEG as described in the main text.

For the first purpose, the dielectric function of the SiO_2 on the top layer had to be slightly modified. This can be justified by the different methods of film formation: the substrate SiO_2 was formed by thermal deposition, whereas the top layer was deposited by e-beam evapo-

ration. Fig. S1 shows the different SiO_2 dielectric functions. It is observed that the evaporated film (solid line), although not identical, shares most of the spectral structure with the thermal oxide (dash-dotted line). Some of the resonances resemble more the glass used for microscope slides (dashed line), also shown in Fig. S1. This resemblance of dielectric functions provided confidence for the model.

Cu/ Bi_2O_3 fits

In the following we show experimental ellipsometric angles ψ and Δ together with resulting best fits in the whole working spectral range for Cu/ Bi_2O_3 . They are shown in Figs. S5. It is observed that good quality fits were obtained for both ψ and Δ for the three different Cu thicknesses.

For the model we employed the optical properties for the common substrate as described above, using the dielectric functions of thermal oxide (dashed line in Fig. S1), the corresponding Cu thickness dependent dielectric function form Fig. S3, and the bulk-like Bi_2O_3 optical response in Fig. S2 for the top layer. The optical properties of the 2DEG were set as fitting parameters in an iterative way by taking into account the minimization of the mean-square error, the spectral structure (Experimental minus modeled spectra) of absolute error and consistency between all three samples.

In Fig. S5(c) we have included a second Fano resonance at around 370 meV, which is also shown in the analysis of 50 nm Cu Bi_2O_3 in Fig. 6 in the main text. Work to find its physical significance is in progress. Although this structure seems not visible for the samples with other underlying Cu thicknesses, it can actually be revealed by analyzing the absolute error of the fit: In Fig. S5(b) we show the fit without including this second Fano resonance for the 20 nm Cu sample. Subtraction of the fit from the experiment, shown in Fig. S6, reveals a structure at the same position, 366 meV, as the second Fano resonance in the 50 Cu sample.

In order to reduce uncertainty concerning the proposed 2DEG layer at the Cu/ Bi_2O_3 interface, we probed the possibility of artificially obtaining a layer with special features at the Cu/ SiO_2 interface. To this end, we introduced a new layer in the model of the reference samples as depicted in the schematic drawing in Fig. S7. The position of this layer was varied vertically but its thickness was kept constant at 5 nm. The thicknesses of the Cu and SiO_2 layers were adapted accordingly. For each layer position, an assumption-free point-by-point fitting procedure delivered a dielectric function which was afterwards parameterized. This resulted in a combination of Cu and SiO_2 dielectric functions with different weights according to the layer position, i.e., an effective medium approximation (EMA). The Cu DF is the one corresponding to

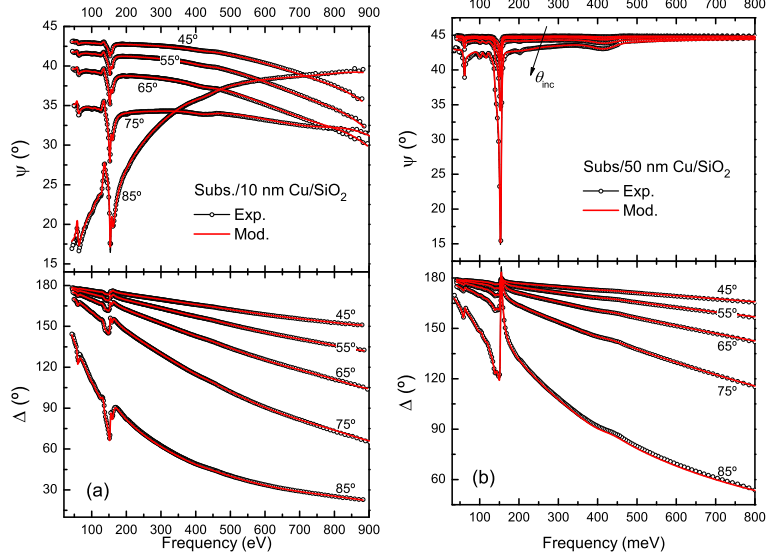


FIG. S4. Experimental and modeled ellipsometric angles ψ and Δ for the SiO_2 layer on (a) 10 nm Cu and (b) 50 nm Cu, recorded at the indicated angles of incidence. θ_{inc} at the top panel in (b) spans the same angles of incidence as all the other panels. “Subs” in the legends stands for the $\text{Si}(001)/320$ nm SiO_2 substrate.

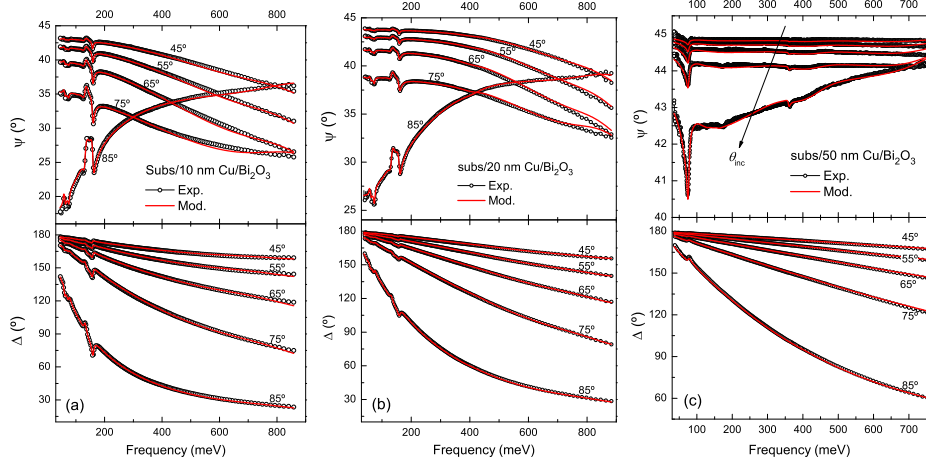


FIG. S5. Experimental and modeled ellipsometric angles ψ and Δ for the Bi_2O_3 layer on (a) 10 nm Cu, (b) 20 nm Cu, and (c) 50 nm Cu.

the 50 nm thick layer. In other words, we obtained dielectric functions of a conducting layer whose conductance is diminished by the influence of the insulating component, but whose characteristic lifetime is preserved. This is shown in Fig. S7 through an Ordal analysis [4], in which the negative of the real and the imaginary parts of the DF are plotted in a log-log graph. The energy of the crossing point gives the lifetime and its height gives the plasmon frequency. From those, the DC conductivity can be extracted as in the common Drude line shape. The circles in Fig. S7 indicate that no alterations of lifetime can be induced by an erroneous assumption of the artificial layer. The resulting ψ spectra were all very similar to the experiment, and thus not shown here, and the fitting

error increased with the vertical position of the artificial layer. To emphasize the compositional character of this artificial layer we also show the first energy derivative of the real part, which tends to enhance spectral structures. SiO_2 features are indicated with arrows. The equal curvatures of all spectra at the lower frequencies side is also a nice indication of a preserved characteristic lifetime. Furthermore, the fact that the *enhanced* spectra run parallel for the different artificial layer positions indicates that no other spectral peaks or “special features” can be unintendedly obtained by misusing an effective medium approximation. Another possibility that might explain the line shape of the $\text{Cu}/\text{Bi}_2\text{O}_3$ interface DF concerns a different chemical composition of the such a layer

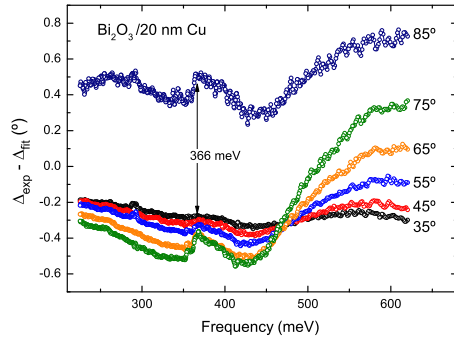


FIG. S6. Absolute error (Experiment – Model) in Δ for the $\text{Bi}_2\text{O}_3/20$ nm Cu sample around the 366 meV feature. Note that the error is well within a $\pm 1^\circ$ range, and that the aforementioned peak amplitude depends on the angle of incidence.

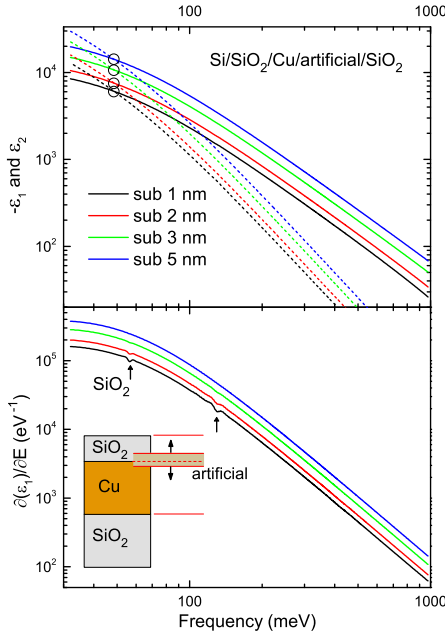


FIG. S7. Log-log plots of the dielectric functions of an artificial layer inserted at different locations, as represented in the schematic diagram, in the SiO_2 reference samples model. The labels *sub* in nm indicate the fraction of the artificial layer below the original interface (dotted line). (Top) Ordal's analysis [4] for the real (solid lines) and imaginary (dashed lines) parts of the DF of the inserted layer. The circles enclose the crossing points: The lifetime of the conduction electron in this layer is the same for all the shown combinations. (Bottom) First energy derivative of ϵ_1 used to enhance structure and evaluate curvature, since it provides an estimation of life times.

as discussed below.

In Fig. S8 we present simulations of ψ spectra corresponding to 50 nm Cu/ Bi_2O_3 in which the interfacial layer has been substituted either by a medium consisting of Cu_2O or by an effective medium composed of a mixture of Cu_2O and Cu. The overall spectra reproduce reasonably well the experiment when the underlying Cu

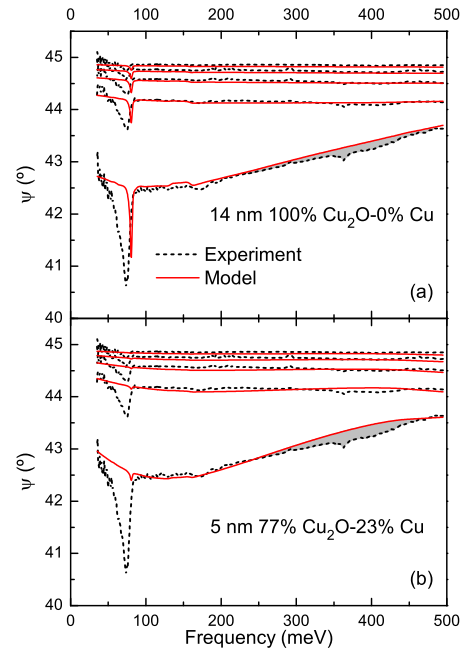


FIG. S8. Simulated ψ -spectra in which the interfacial layer is composed of either Cu_2O (a) or an effective medium of Cu_2O and Cu (b). To achieve resemblance to experiment the underlying Cu thickness had to be modified as well. The shaded area indicates the place of the SOC_2 resonance which is better simulated by the 2DEG model.

film thickness is increased to 55 nm. The artificial layer thicknesses are 5 nm and 14 nm for the EMA and the pure Cu_2O , respectively. In both cases the Bi_2O_3 thickness is greatly reduced to 4.5 and 13 nm, respectively. These simulated Bi_2O_3 thicknesses are at odds with our TEM measurements (a separate manuscript is in preparation). None of the cases of a dielectric layer with resonances in the present range was able to reproduce the characteristics of the 2DEG-SOC layer, except if assuming unrealistic thicknesses, such as the sharp peak at ~ 100 meV in Fig. S8(a). As an example, in Fig. S8(a) and (b) we emphasize with a gray shade the difference between models and experiment at the region where we claim SOC_2 is located. However, there is a valuable piece of information: some small features in the range of 130 to 200 meV in the form of wiggles in the experiment, which are not well reproduced by our official simulations [see Fig. 2(b) in the main text] are somehow incipiently reproduced for the pure Cu_2O layer. This might provide a hint at the nature of bonds at the interface. However more work needs to be done to answer this issue.

Finally, we present a graphical depiction of the free electron data of the 2DEG in Table I (in the main text) in Fig. S9 together with the thickness dependent Cu DF. To this end, we also make use of the Ordal analysis [4]. The main part of the figure shows the free-electron contributions to the DF of the 2DEG forming at the 50 nm

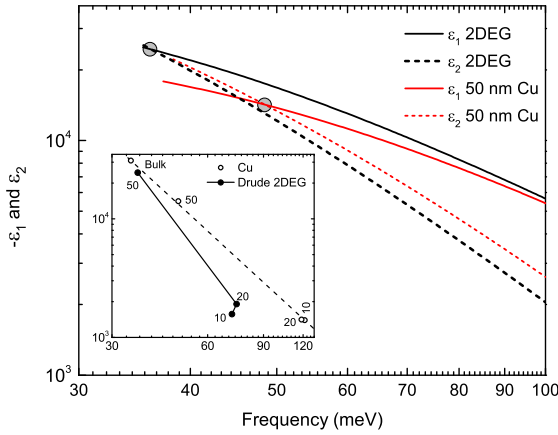


FIG. S9. Crossing-point analyses (gray symbols) of 50 nm Cu layer (red lines) and the free electron contribution to the 2DEG layer forming at the 50 nm Cu/Bi₂O₃ interface (black lines). The inset shows the resulting crossing points for the different Cu layers (hollow symbols) and the corresponding free electron contributions to the 2DEG's for all Cu/Bi₂O₃ samples (black symbols), where the Cu thickness (in nm) is used as parameter. The dashed line connecting Cu points is for visual aid.

Cu/Bi₂O₃ interface (black lines) and that of the underlying Cu film (red lines). It is observed that both the conductivity and the characteristic lifetimes are quite different (crossings indicated with grey circles). Such differences, as discussed in the context of Fig. S7 cannot be produced by an artifact of an overlooked effect

tive medium approximation. In the inset of Fig. S9 we collect data for all samples. The thickness dependent free-electron Cu characteristic data fall in a line as if it were parametrically constructed with the Cu thickness (dashed line in the inset). However, we cannot extract any physical meaning from this since the Cu thickness spacing, i.e., the partition of the line, does not seem to show any regularity. The free-electron characteristics of the 2DEG layer, on the other hand, follow its corresponding underlayer Cu but always at the longer lifetime side of the Cu line, indicating that the 2DEG electron density critically depends on the Cu capacity of sharing charge as a function of its thickness as discussed in the main text. Furthermore, the 2DEG does not show the apparent regularity of the Cu layers, however this can be explained in terms of stressed/relaxed regimes at the interface.

* e-mail: jmflores@cactus.iico.uaslp.mx

† e-mail: jorgeluis.pueblanunez@riken.jp

- [1] M. Hövel, B. Gompf, and M. Dressel, Phys. Rev. B **81**, 035402 (2010).
- [2] N. Smith, Phys. Rev. B **64**, 155106 (2001).
- [3] E. D. Palik, *Handbook of Optical Constants of Solids* (Academic Press, 1985).
- [4] M. A. Ordal, L. L. Long, R. J. Bell, S. E. Bell, R. R. Bell, J. R. W. Alexander, and C. A. Ward, Appl. Opt. **22**, 1099 (1983).